ESC European Society of Cardiology

European Heart Journal Open (2022) **2**, 1–16
https://doi.org/10.1093/ehjopen/oeac047

ORIGINAL ARTICLE
Translational basic science

Vascular senescence in progeria: role of endothelial dysfunction

Qiu Xu [1,2,†], Anahita Mojiri[1,†], Luay Boulahouache [1], Elisa Morales [1], Brandon K. Walther [1], and John P. Cooke [1,*]

[1]Department of Cardiovascular Sciences, Center for Cardiovascular Regeneration, Houston Methodist Research Institute, Houston 77030, TX, USA; and [2]Department of Neurology, Xiangya Hospital, Central South University, Changsha 410008, China

Received 27 September 2021; revised 2 June 2022; accepted 25 July 2022; online publish-ahead-of-print 28 July 2022

Handling Editor: Marie-Luce Bochaton-Piallat

Aims Hutchinson–Gilford progeria syndrome (HGPS) is a pre-mature aging disorder caused by the mutation of the LMNA gene leading to an irreversibly farnesylated lamin A protein: progerin. The major causes of death in HGPS are coronary and arterial occlusive disease. In the murine model of HGPS, vascular smooth muscle cell (VSMC) loss is the primary vascular manifestation, which is different from the arterial occlusive disease seen in older patients.

Methods and results To identify the mechanisms of HGPS vascular disease in humans, we differentiated isogenic endothelial cells (ECs) and VSMCs from HGPS-induced pluripotent stem cells (iPSCs) and control-iPSCs. Both HGPS-ECs and HGPS-VSMCs manifested cellular hallmarks of aging, including dysmorphic nuclei, impaired proliferation, increased β-galactosidase staining, shortened telomeres, up-regulated secretion of inflammatory cytokines, increased DNA damage, loss of heterochromatin, and altered shelterin protein complex (SPC) expression. However, at similar days after differentiation, even with lower levels of progerin, HGPS-ECs manifested more severe signs of senescence, as indicated in part by a higher percentage of β-galactosidase positive cells, shorter telomere length, and more DNA damage signals. We observed increased γH2A.X binding to RAP1 and reduced TRF2 binding to lamin A in HGPS-ECs but not in HGPS-VSMCs. The expression of γH2A.X was greater in HGPS-ECs than in HGPS-VSMCs and is associated with greater telomere shortening, impaired SPC interactions, and loss of heterochromatin.

Conclusion Although progerin expression has a deleterious effect on both ECs and VSMCs, the dysfunction is greater in HGPS-ECs compared with HGPS-VSMCs. This study suggests that an endothelial-targeted therapy may be useful for HGPS patients.

* Corresponding author. Tel: 1 713 441 8322, Email: jpcooke@houstonmethodist.org
† The first two authors contributed equally to the study.

Graphical Abstract

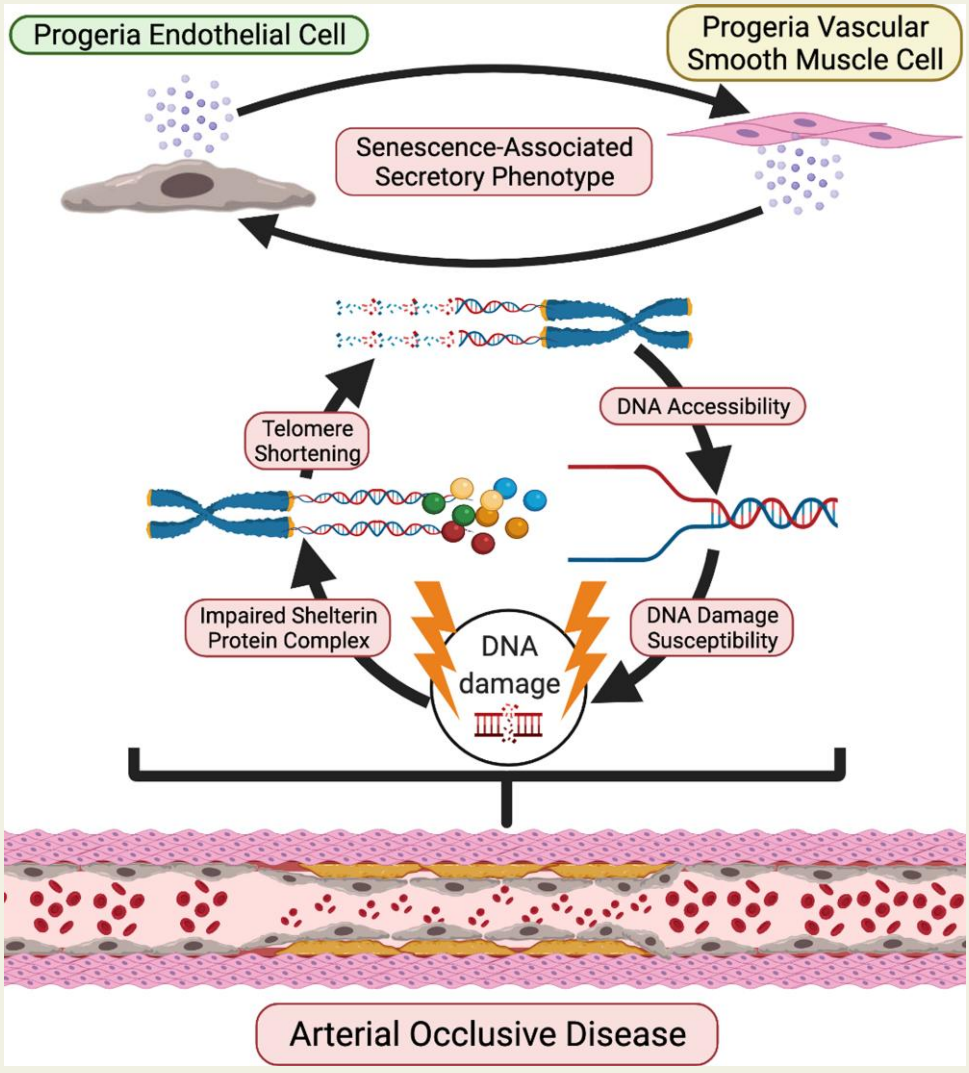

A schematic figure of phenotypes for progeria endothelial cells (ECs) and vascular smooth muscle cell (VSMCs). Both HGPS-ECs and HGPS-VSMCs exhibit increased inflammatory cytokine expression, impaired shelterin complex proteins, shortened telomeres, increased DNA damage, and greater DNA accessibility. However, DNA accessibility and telomere shortening are far more severe in HGPS-ECs, suggesting an important role in the initiation and progression of the arterial occlusive disease in progeria.

Keywords Progeria • iPSCs • Endothelial cells • Vascular smooth muscle cells • Senescence • Telomere

Translational Perspective

Coronary and carotid artery disease is accelerated in progeria and causes death from heart attack and stroke at an early age. This study reveals that a disproportionate dysfunction in the endothelium may play a role in the progression of the arterial occlusive disease in progeria. Accordingly, endothelial-targeted therapies may be useful for ameliorating cardiovascular disease in these patients.

Introduction

Hutchinson–Gilford progeria syndrome (HGPS) is a rare pre-mature aging disorder caused by a *de novo* heterozygous silent mutation (c.1824C > T; p.G608G) in exon 11 of LMNA.[1] The *de novo* mutation activates a cryptic splice site, causing a 50 amino acid deletion, yielding a permanently farnesylated protein known as progerin, which localizes at the nuclear envelope.[1,2] Progerin affects a gamut of cellular functions, gene expressions, heterochromatin organization, DNA repair, and nuclear architecture.[3,4] Initially, HGPS patients appear

normal at birth, but progressively, the cellular changes accumulate, leading to severe growth abnormalities, and severe skin changes occur within the first years of life.[5] The clinical presentation includes alopecia, loss of body fat, bone and joint abnormalities, and severe vascular disease with death in the teen years due to myocardial infarction and stroke.[6,7]

Although attenuation of the media is observed in proximity to extensive overlying intimal lesions in atherosclerosis, in HGPS, there is a disproportionate loss of vascular smooth muscle cells (VSMCs) in the conduit vessels, even in the absence of severe intimal thickening.[8,9] Furthermore, in HGPS murine models, there is a prominent loss of VSMCs in the aortic media. Indeed, the first report describing the most widely used murine model of HGPS highlighted the loss of VSMCs, stating that the model '…does demonstrate the progressive vascular abnormalities that closely resemble the most lethal aspect of the human phenotype.' (Varga *et al.*, 2006). However, this mouse model *does not* in fact phenocopy the arterial occlusive disease that causes cardiovascular death in HGPS. Nevertheless, these observations have led most investigators in the field to focus on the effects of progerin on VSMC biology.[10–12] However, the loss of VSMCs does not seem to contribute directly to cardiovascular morbidity or mortality in HGPS patients. Specifically, in patients, the media is replaced in part by collagen and extracellular matrix, with no evidence of ectasia or aneurysm formation (Stehbens, Delahunt, Shozawa, & Gilbert-Barness, 2001; Stehbens, Wakefield, Gilbert-Barness, Olson, & Ackerman, 1999) that might cause a vascular catastrophe.

The focus on VSMCs looks past the finding that in humans, the mortality in progeria is due to coronary and carotid occlusive disease, not a deficiency of VSMCs in the media. Furthermore, there is an incongruous dearth of investigations into endothelial biology as a contributor to the arterial occlusive disease in progeria. Endothelial dysfunction is the first observable abnormality in experimental atherosclerosis; promotes the initiation and progression of vascular disease; and is associated with major adverse cardiovascular events in humans.[13,14] Subsequently, monocyte infiltration and foam cell formation, together with VSMCs proliferation, causes occlusive disease.[15]

In our prior study, we showed that HGPS had deleterious effects on endothelial cells (ECs) that could be reversed by mRNA telomerase. In the current paper, we show that EC dysfunction is more severe than the VSMC defect in HGPS. This is an important point to make, as the community of scientists working on HGPS is largely focused on VSMC deficiency. Our new data support the view that the focus of our scientific community should be on the endothelium because of the greater role of the endothelium in vascular homeostasis and the greater deficit of this tissue in HGPS. A redirection of our scientific efforts may guide well-targeted and successful therapies for HGPS patients. Hence, in view of the key role that the endothelium plays in other vascular diseases, in this study, we have performed the first head-to-head comparison of the cellular dysfunction in human endothelial and vascular smooth muscle cells using induced pluripotent stem cell (iPSC)-derived vascular cells from an HGPS patient and their unaffected parent. Our work indicates that HGPS has detrimental effects on both ECs and VSMCs, but the dysfunction is more extensive in HGPS-ECs in comparison with HGPS-VSMCs with respect to telomere length, senescence markers, and DNA damage. These results support the primacy of an EC dysfunction in HGPS vascular disease.

Methods

Cell culture

Control iPSCs (HGFDFN168 iPSC1P) and HGPS iPSCs (HGADFN167 iPSC1Q) were purchased from the Progeria Research Foundation (PRF) Cell and Tissue Bank and cultured in mTeSR plus medium (STEMCELL Technologies) on Matrigel-coated (BD Biosciences) plates (Corning). For maintenance, iPSCs were passaged at 80% confluency and media was changed every day. ECs and VSMCs were differentiated from iPSCs using established protocols with minor changes.[17,18] Briefly, for EC differentiation, iPSCs were seeded in 100 × 20 mm tissue culture Matrigel-coated plates (Corning) cultured with mesodermal media for 3 days. On Day 3, the cells were detached and reseeded in a ratio of approximately 1:15 to plates with endothelial differentiation media for 4 days. On Day 7, cells were cultured in endothelial maturation media composed of EGM-2MV media (Lonza) and 100 ng/ml vascular endothelial growth factor (VEGF) for 4 days. On Days 10–12, ECs were isolated by fluorescence-activated cell sorting (FACS) with CD31 (Alexa Fluor 488-conjugated antibody, BD Pharminogen) and CD144 (PE-conjugated antibody, BD Pharminogen). The sorted ECs were cultured in endothelial growth media (EGM-2, Lonza) supplemented with 1% penicillin/streptomycin (Gibco), and media was changed every other day. The ECs were collected on Days 13–16 (Passages 0–2) for the experiments. For VSMC differentiation, embryoid bodies (EBs) were generated from iPSC colonies and plated on 6-well low-cluster plates (Corning) for 7–10 days. On Day 10, EBs were transferred to Matrigel-coated 6-well plates in E6 media (StemCell Technologies #05946) with supplement (StemCell Technologies #05948) for 5–8 days. EBs were trypsinized to single cells and plated on Matrigel-coated 6-well plates with smooth muscle cell medium 231 (M231500, Thermo Fisher Scientific) supplemented with smooth muscle cell growth supplement (S00725, Thermo Fisher Scientific). When cells reached 80% confluency, they were passaged from one well to three wells in a 1:3 ratio and grown for around 10 days to become mature VSMCs. The VSMCs were collected on Days 35–40 (Passages 2–4) for the experiments.

Quantitative reverse transcription polymerase chain reaction

Total RNA was extracted by using RNeasy Plus Mini kit (Qiagen #74136) according to the manufacturer's protocol. The mRNA was reverse-transcribed into cDNA using iScript cDNA Synthesis kit (Bio-Rad #1708841). Quantitative reverse transcription polymerase chain reaction (RT-qPCR) was performed by using QuantStudio 12K Flex (Applied Biosystems, Life Technologies). Predesigned primers including CNN1, ACTA2, MYH11, TAGLN (Qiagen), TRF1, TRF2, TIN2, POT1, and TPP1 (Bio-Rad) were used. Custom-designed primers including RAP1, IL-1β, IL-6, IL-10, TNF-α, ICAM1, VCAM1, MCP1, M-CSF, GM-CSF, and β-actin primers were designed based on the literature.[19]

Immunofluorescence staining

ECs and VSMCs were fixed with 4% paraformaldehyde and washed three times. The cells were blocked with a blocking buffer including 2% bovine serum albumin (BSA; Fisher Scientific #BP9706-100) and

0.2% Tween 20 (Sigma-Aldrich) for 1 h at room temperature, and primary antibodies were added to the cells overnight at 4°C. The following day, the cells were washed three times. The cells were incubated with secondary antibodies (anti-rabbit Alexa-488 and anti-rat Alexa-555, Thermofisher) for 1 h at room temperature and then washed with PBS. Slides were mounted with 4′,6-diamidino-2-phenylindole (DAPI). Pictures were taken by using the FluoView FV3000 confocal microscope. Primary antibodies included the following: Smoothelin (Abcam #ab204305), α-smooth muscle actin (Abcam), CD144 (Biosciences #555661), VWF (citeab #A0082), Lamin A (Invitrogen #MA1-06101), γH2A (Millipore #05-636), 53BP1 (Novus #NB100-304), histone H1 (Abcam #ab61177), and HP1α (Cell Signalling #2616s). γH2A.X and 53BP1 were reported for colocalization. Fluorescence intensity for histone H1 and HP1α were normalized with nuclei area.

Quantitative fluorescent *in situ* hybridization

Cells were arrested at metaphase by adding colcemid at a concentration of 0.1 ug/ml to ECs for 2 h and VSMCs overnight. The cells were harvested and placed in a test tube. While vortexing at a low speed, 4 ml of a hypotonic solution (50 mM KCl, Sigma-Aldrich) was added drop wise. The cells were then incubated at 37°C for 30 min followed by a fixative solution of 3:1 ethanol/acetic acid. The cells were centrifuged for 5 min at 1000 rpm. The fixation step was repeated again and the supernatant was removed after centrifuge. The fixed cells were dropped on slides and the slides were fixed with 3.7% formaldehyde and washed with PBS three times. The slides were dehydrated in ethanol in a series of 70%, 85%, and 100% for 5 min each. Hybridization buffer (HB) and the slides were heated on a heater (85°C) for 5 min. Telomere probe (PNA Bio F1013 TelC-Alexa 647) was then diluted into HB (1:40) and heated for another 5 min. The telomere probe plus the HB mixture were added to each slide. The slides were covered with a coverslip and heated for 10 min at 85°C for denaturation. Afterwards, the slides were left overnight at 4°C in a humidified chamber away from light. The next day, the slides were washed with wash buffer #1 (70% Formamide, Tris 20 mM pH 7.5, BSA 1%) and then with wash buffer #2 (Tris 50 mM pH 7.5, NaCl 150 mM, Tween 20 0.05%). Next, the slides were dehydrated in an ethanol series of 70%, 85%, and 100% for 5 min each and finally mounted with DAPI. Pictures were taken with the FluoView FV3000 confocal microscope. Telomere length was measured as the intensity of the telomere probe normalized to the intensity of DAPI or nuclei area.

Real-time proliferation assay

Real-time proliferation assay was performed using the xCELLigence instrument (Roche). For each 16-well E-plate (Agilent #5469830001), 3000 ECs and VSMCs from control and HGPS were seeded into each well, triplicated for each group, and incubated at 37°C. The impedance value of each well was monitored every 15 min for a total of 160 h and expressed as a Cell Index value. For counting cells within 10 days, 20 000 control-ECs and HGPS-ECs were seeded in 24-well plates and 20 000 control-VSMCs and HGPS-VSMCs were seeded in 12-well plates on Day 0. Cell number was counted every other day: Days 2, 4, 6, 8, and 10. Cell number and time curve were generated within 10 days.

β-galactosidase staining

According to the manufacturer's instructions (Cell Signalling #9860), media was removed from cells, and plates were rinsed once with PBS. The cells were fixed using fixative solution (provided by the kit) for 12 min at RT followed by washing PBS twice. Next, 1 ml of the β-galactosidase staining solution was added to each 35 mm well. The plates were sealed and incubated at 37°C overnight in a dry incubator without CO_2. The cells were analysed using an RGB microscope by quantifying the number of blue cells. For each experiment, at least 300 cells were counted for each group.

Bio-Plex assay

A Bio-Plex assay composed of 48 inflammatory markers was conducted using a Bio-Rad kit (Bio-Rad #12007283). Control-VSMCs and HGPS-VSMCs were collected and lysed. A total of 750 μg/ml of each sample was used in triplicate and incubated with magnetic beads conjugated to antibodies. The beads were washed in a plate and incubated on a shaker for 30 min at RT. After incubation, detection antibody was added and the samples were incubated on the shaker for 30 min at RT. The beads were washed again, and then SA-PE was added and incubated on the shaker for 10 min at RT. Finally, the beads were washed and resuspended in an assay buffer for 30 s. Data were acquired using the Bio-Plex System.

Western blot

The cells were lysed in a lysis buffer (Thermo Scientific #89900) with protease inhibitor (Roche #11836180001) and phosphatase inhibitor (Thermo Scientific #1861281), and the cell lysate was spun at the highest speed for 10 min. After measuring protein using a DC protein assay, 20 μg of each sample was prepared using a 4 × sample buffer (Bio-Rad #1610747) and heated for 10 min. The samples were loaded and resolved in TGX Stain-Free gel (Bio-Rad). After transferring to the nitrocellulose or PVDF membranes (Bio-Rad) using the Bio-Rad transfer system, the membranes were blocked in a Clean Western Buffer (KwikQuant #R2001) for 1 h. The membranes were incubated overnight at 4°C with primary antibodies. The next day, the membranes were washed with the Clean Western Buffer three times for 15 min each. Afterwards, the samples were incubated for 1 h at room temperature with secondary horseradish peroxidase-label anti-mouse or anti-rabbit antibody (KwikQuant #R1004). Then, the membranes were washed three times with the Clean Western Buffer for 15 min each. Visualization and image acquisition were done with a Fujifilm Corporation digital camera (KwikQuant). Densitometry data were analysed by using Image-J software. Primary antibodies included the following: progerin (Abcam #ab66587), histone H1 (Abcam #61177), HP1α (Cell Signalling #2616s), TRF1 (Novus #NB110-68281), TRF2 (Novus #NB110-57130), TIN2 (Abcam #ab197894), RAP1 (Abcam #ab14404), POT1 (Proteintech #10581-1-AP), TPP1 (Cell Signalling #4667), γH2A (Abcam #ab81299), Lamin A (Invitrogen #MA1-06101), P16 (Abcam #ab108349), P21 (Abcam #ab109520), and tubulin (Cell Signalling #86298).

Immunoprecipitation

Cells were lysed with NP-40 (GenDEPOT #N1200-050) plus protease inhibitor and phosphatase inhibitor by sonication (Diagenode). Protein levels were measured with a DC protein assay. Each sample with 1000 μg in 500 μl was precleared using 40 μl protein A/G PLUS agarose (Santa Cruz, sc-2003) and incubated for 30 min with gentle agitation. Using a magnetic stand, the samples were cleared from the beads and the supernatant were transferred to a new tube and incubated with 2–5 μg of antibody per sample and incubated overnight at 4°C rotating. The next day, 50 μL of agarose beads were added to each sample and incubated for 2 h at 4°C with gentle agitation. The beads were washed with NP-40 three times for 5 min each. The samples were eluted in a sample buffer for western blot analysis. The following primary antibodies were used for immunoprecipitation (IP): anti-mouse IgG (Abcam #ab37355), anti-rabbit IgG (Abcam #ab172730), RAP1 (Abcam #ab14404), γH2A (Abcam #ab81299), and lamin A/C (Abcam #ab108595).

Time-course experiment for ECs and VSMCs

For ECs, we collected control and HGPS cells on Days 7 (Passage 0), 14 (Passages 1–2), 21 (Passages 2–3), and 28 (Passages 3–4) for RT-qPCR to detect mRNA expression for progerin and inflammatory markers. For senescence-associated β-galactosidase (SABG) staining and quantitative fluorescent *in situ* hybridization (qFISH), the cells were collected on Days 8, 14, 21, and 28. On Day 7, the ECs were cultured in endothelial maturation media with 100 ng/ml VEGF. The ECs at other timepoints were cultured in endothelial growth media according to the differentiation protocol. For VSCMs, we collected cells on Days 30 (Passages 0–2), 37 (Passages 2–4), 44 (Passages 4–6), and 51 (Passages 6–8) for RT-qPCR to detect for mRNA expression of progerin and inflammatory markers, SABG staining, and qFISH. The VSMCs were cultured with complete smooth muscle cell medium 231. All cells were incubated at 37°C and 5% CO2.

Mass spectrometry

The control-ECs and HGPS-ECs were collected and processed using the IP procedure to pull down RAP1 protein. The immunoprecipitated samples were transferred to the Baylor BCM Mass Spectrometry Proteomics Core for further analysis. Briefly, the samples were resolved on NuPAGE 10% Bis-Tris Gel (Life Technologies) and processed for in-gel digestion using trypsin enzyme. The tryptic peptides were analysed on the nano-LC 1000 system (Thermo Fisher Scientific, San Jose, CA) coupled to the Orbitrap Fusion™ (Thermo Fisher Scientific, San Jose, CA) mass spectrometer. The peptides were loaded on a two-column setup using a pre-column trap of 2cm × 100μm size (Reprosil-Pur Basic C18 1.9 μm, Dr. Maisch GmbH, Germany) and a 20cm × 75μm analytical column (Reprosil-Pur Basic C18 1.9 μm, Dr. Maisch GmbH, Germany) with a 110 min gradient of 6–30% acetonitrile/0.1% formic acid at a flow rate of 200 nl/min. The eluted peptides were directly electrosprayed into the mass spectrometer operated in the data-dependent acquisition (DDA) with top 35 mode. The full MS scan was acquired in Orbitrap in the range of 300–1400 m/z at a 120 000 resolution followed by MS2 in Ion Trap (HCD 30% collision energy) with a 5-second dynamic exclusion time. The RAW file from the mass spectrometer was processed with Proteome Discoverer 2.1 (Thermo Scientific) using the Mascot 2.4 algorithm (Matrix Science) with percolator against the human protein NCBI refseq (updated 2020_0324). The precursor ion tolerance and product ion tolerance were set to 20 ppm and 0.5 Da, respectively. Dynamic modification of oxidation on methionine, protein N-terminal Acetylation, and destreak on cysteine were allowed. The peptides identified from the mascot result file were validated with a 5% false discovery rate (FDR). The gene product inference and iBAQ-based quantification were carried out using the gpGrouper algorithm (PMID: 30093420). The differentially expressed proteins were calculated using the moderated *t*-test to calculate *P*-values and $\log_2$ fold changes in the R package limma. The FDR-adjusted *P*-value was calculated using the Benjamini–Hochberg procedure.

Statistical analysis

Data were expressed as mean ± standard deviation. $N \geq 3$ for each experiment. A student's *t*-test was applied when comparing two groups, or the analysis of variance test was used when comparing ≥ 3 groups using Graphad PRISM 8 software. A value of $P < 0.05$ was considered statistically significant.

Results

Differentiation and characterization of iPSC-derived ECs and VSMCs

We used iPSCs derived from the fibroblasts of HGPS patients and their unaffected parents, serving as control. The control-iPSC and HGPS-iPSC colonies were indistinguishable under light microscopy (see Supplementary material online, *Figure S1*). We differentiated ECs and VSMCs from the same iPSCs of both HGPS and their unaffected parents using established protocols[17,18] to eliminate inherent genomic differences, thus allowing an accurate comparison of the two cell types (*Figure 1A*). On Day 7, the ECs were isolated by FACS using CD31 antibody. They became mature ECs by Day 14, where they were isolated by FACS using both CD31 and CD144 and stained with VWF and CD144 (see Supplementary material online, *Figure S1*). We previously characterized HGPS-ECs in comparison with the control-ECs. HGPS-ECs displayed significant defects in angiogenesis, reduced nitric oxide (NO) production, and reduced acetylated-LDL uptake.[16,18] Moreover, we previously observed global alterations in gene expression associated with increased inflammatory cytokines and reduced expression of EC identity genes.[16]

VSMCs were differentiated from iPSCs for a period of 30 days and identified by the expression of α-smooth muscle actin and smoothelin (*Figure 1B*). We further characterized vascular gene expression using VSMC markers: CNN1, ACTA2, MYH11, and TAGLN. These markers were present, albeit reduced in HGPS-VSMCs compared with control-VSMCs (*Figure 1C*). While HGPS-VSMCs were morphologically indistinguishable from control-VSMCs (*Figure 1D*), HGPS-ECs were morphologically distinct from control-ECs. Specifically, they displayed typical features of senescent ECs, i.e. a more circular shape[18] with a greater surface area, and a central prominent nucleus, the classical 'fried egg' appearance of aged ECs (*Figure 1D*). In conclusion, both HGPS-ECs and HGPS-VSMCs

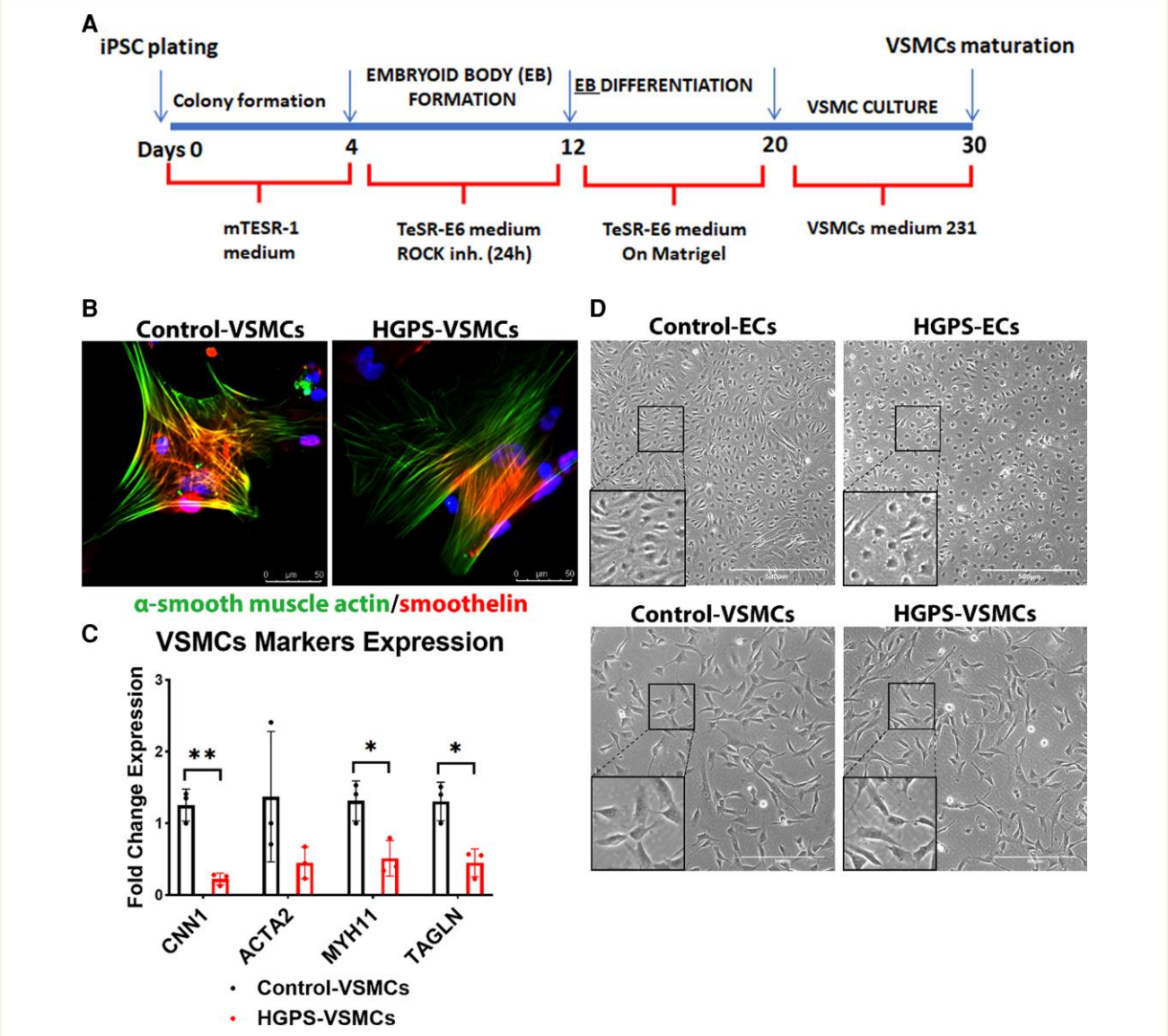

Figure 1 Differentiation and characterization of induced pluripotent stem cells-derived endothelial cells and vascular smooth muscle cells. (*A*) Schematic of the methodology used to differentiate induced pluripotent stem cells into vascular smooth muscle cells. (*B*) Immunofluorescence staining of smooth muscle cells specific markers: smoothelin and α-smooth muscle actin from control-VSMCs and HGPS-VSMCs (scale bar: 50 μm). (*C*) Quantitative reverse transcription polymerase chain reaction for vascular smooth muscle cell marker expression: CNN1, ACTA2, MYH11, and TAGLN after differentiation in control-VSMCs and HGPS-VSMCs. $n = 3$. (*D*) Brightfield images of endothelial cells (scale bar: 500 μm) and vascular smooth muscle cells (scale bar: 300 μm) in both control and Hutchinson–Gilford progeria syndrome groups after differentiation. Statistical analysis was performed by an unpaired *t*-test when comparing two groups. A value of $P < 0.05$ was considered statistically significant. *$P < 0.05$; **$P < 0.01$.

manifested typical markers of their cell identity, although the expression of their markers were attenuated. As opposed to HGPS-VSMCs, HGPS-ECs displayed morphological signs of senescence as early as 14 days following HGPS-iPSC differentiation.

Progerin causes senescence phenotype in both ECs and VSMCs of HGPS

Progerin levels (mRNA and protein) were markedly increased in both HGPS-ECs and HGPS-VSMCs in comparison with the control cells, with a higher expression in HGPS-VSMCs compared with HGPS-ECs (*Figure 2A–C*; see Supplementary material online, *Figure S2*). Aggregation of progerin under the nuclear membrane is thought to cause abnormalities in nuclear morphology.[20] Immunofluorescence (IF) staining for lamin A indicated that both HGPS-ECs and HGPS-VSMCs had significantly increased abnormal nuclei compared with their respective controls (Control-ECs 34.3% vs. HGPS-ECs 74.1%; Control-VSMCs 30.9% vs. HGPS-VSMCs 85.1%; *Figure 2D–E*). After identifying the abnormal nuclei, we compared telomere lengths between the two cell types because telomere attrition is a hallmark of senescence.[21, 22] An impaired interaction with lamin A is thought to accelerate telomere

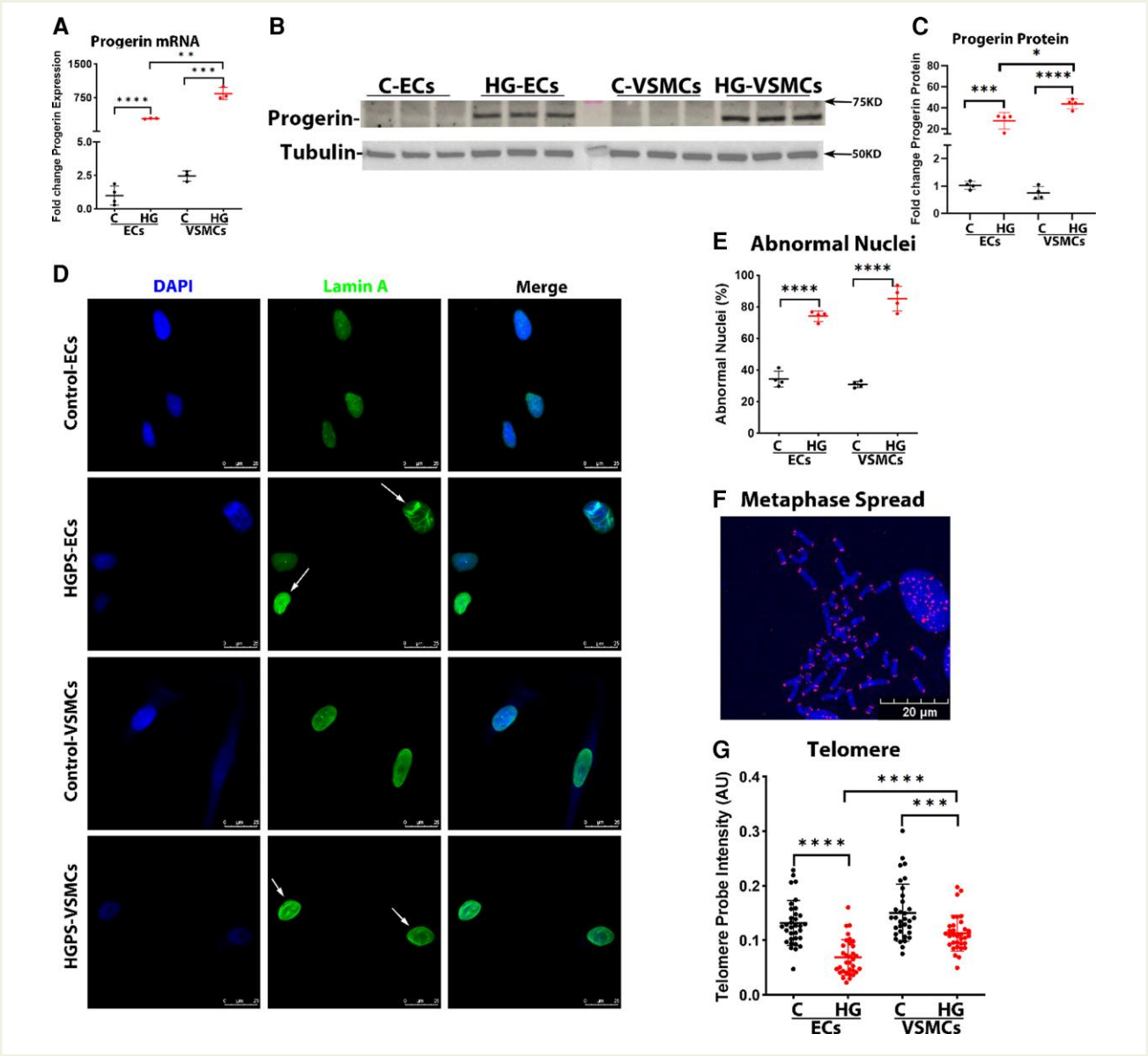

Figure 2 Progerin causes senescence phenotype in both endothelial cells and vascular smooth muscle cells of Hutchinson–Gilford progeria syndrome. (*A*) Quantitative reverse transcription polymerase chain reaction for progerin expression in endothelial cells and vascular smooth muscle cells. $n = 4$ for control-ECs, and $n = 3$ for other groups. (*B and C*) Western blot and its quantification of progerin level in endothelial cells and vascular smooth muscle cells. $n = 4$. (*D*) Immunofluorescence staining of lamin A for nuclear morphology and quantification in (*E*); the white arrows represent abnormal nuclei. $n = 4$. (*F*) A representative figure of metaphase spread (blue: DAPI nucleus, red: cy5 telomere, scale bar: 20 μm). (*G*) Telomere probe intensities were normalized with the DAPI signal for both endothelial cells and vascular smooth muscle cells, $n = 33$ metaphase spread for each group, replicated at least three times. (*H*) Real-time cell proliferation using xCELLigence measured by impedance for both endothelial cells and vascular smooth muscle cells from control and Hutchinson–Gilford progeria syndrome. $n = 4$, replicated three times. (*I and J*) Increased β-galactosidase staining in both HGPS-ECs and HGPS-VSMCs compared with respective controls, with an especially higher percentage in HGPS-ECs among all groups (scale bar: 300 μm) $n = 5$ for HGPS-ECs, $n = 4$ for other groups. (*K*) Quantitative reverse transcription polymerase chain reaction for P16 and P21 expression in endothelial cells and vascular smooth muscle cells. $n = 5$. (*L and M*) Western blot and its quantification of P16 and P21 levels in endothelial cells and vascular smooth muscle cells. $n = 6$–9. C, control; HGPS, Hutchinson–Gilford progeria syndrome. Statistical analysis was performed by an unpaired *t*-test when comparing two groups. A value of $P < 0.05$ was considered statistically significant. *$P < 0.05$; **$P < 0.01$; ***$P < 0.001$; ****$P < 0.0001$.

erosion in HGPS.[23] Monochrome Multiplex quantitative PCR (MMqPCR) revealed a reduction in telomere length in both HGPS-ECs and HGPS-VSMCs (see Supplementary material online, *Figure S3*). We confirmed these results by qFISH using the PNA telomeric probe. Notably, HGPS-ECs had shorter telomeres than HGPS-VSMCs (*Figure 2F and G*). Subsequently, to assess cell

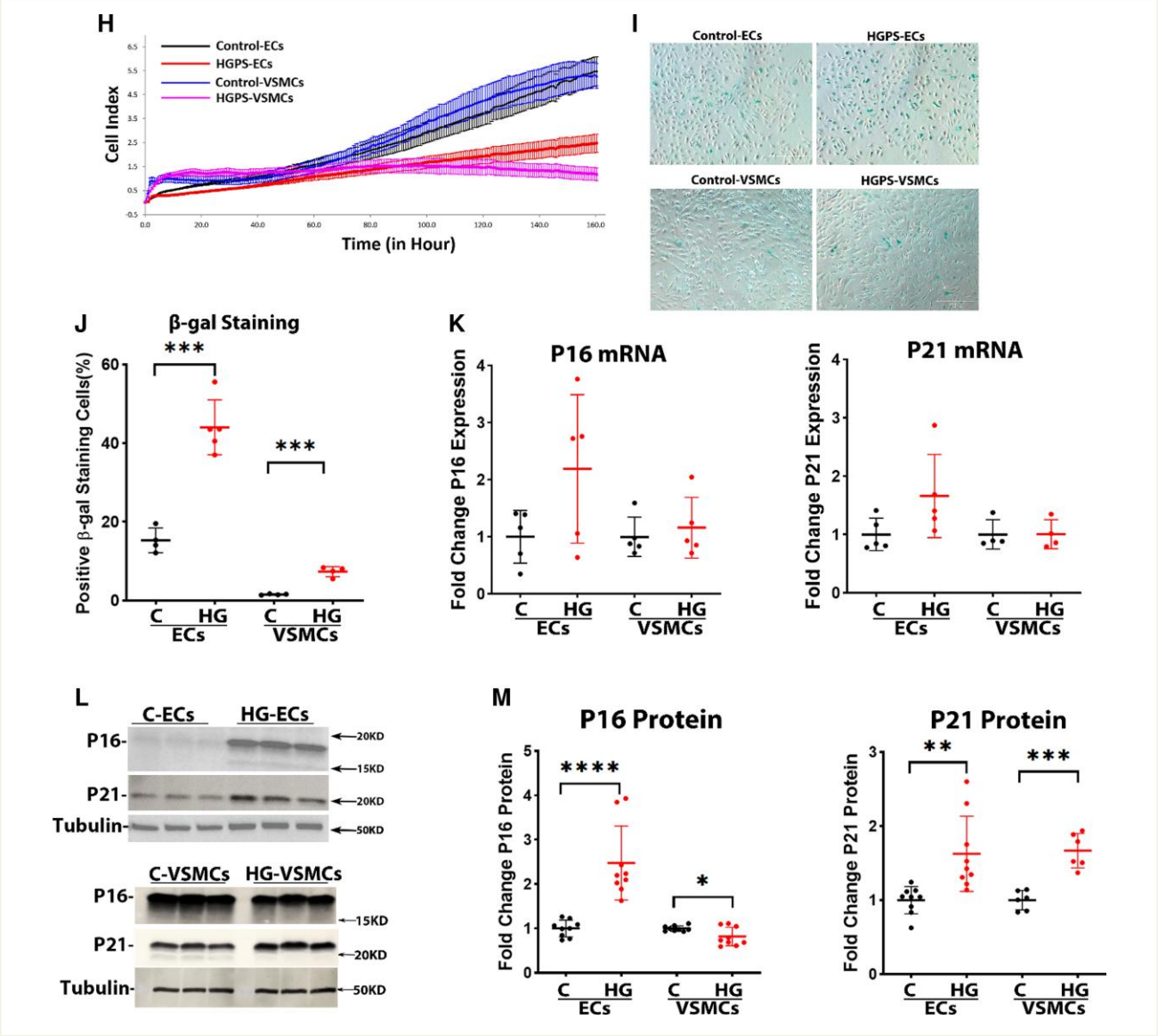

Figure 2 Continued

proliferation, we used xCELLigence and found that both HGPS-ECs and HGPS-VSMCs grew at a significantly lower rate compared with their respective controls (*Figure 2H*). Furthermore, SABG, a marker of cellular senescence,[24] was increased in both HGPS-ECs and HGPS-VSMCs. Notably, β-gal was higher in HGPS-ECs compared with HGPS-VSMCs (Control-ECs 15.3% vs. HGPS-ECs 44.0%; Control-VSMCs 1.5% vs. HGPS-VSMCs 7.4%; *Figure. 2I and J*). Senescence was also studied using two well-known senescent markers, p16 and p21. These two senescent markers were not significantly changed in mRNA expression in both HGPS-ECs and HGPS-VSMCs compared with their respective controls (*Figure 2K*). However, the protein levels of both p16 and p21 increased in HGPS-ECs compared with its control. Surprisingly, p16 did not match a corresponding increase with p21 and instead was reduced in HGPS-VSMCs compared with its control (*Figure 2L and M*). In conclusion, although both HGPS-ECs and HGPS-VSMCs manifested the characteristics of senescence, telomere erosion and β-gal staining were greater in HGPS-ECs than in HGPS-VSMCs.

DNA Damage, inflammation, and DNA accessibility in ECs vs. VSMCs

Genomic instability, as a result of DNA damage, is closely related to aging.[25,26] Prior work has provided evidence for increased DNA damage in HGPS fibroblasts,[17] VSMCs,[27] and ECs.[16,17] We assessed DNA damage using IF staining and quantified colocalization of DNA damage markers: γH2A.X and 53BP1. Clear evidence of DNA damage was observed in HGPS-ECs. However, in HGPS-VSMCs, the evidence for DNA damage was not as strong (*Figure 3A and B*).

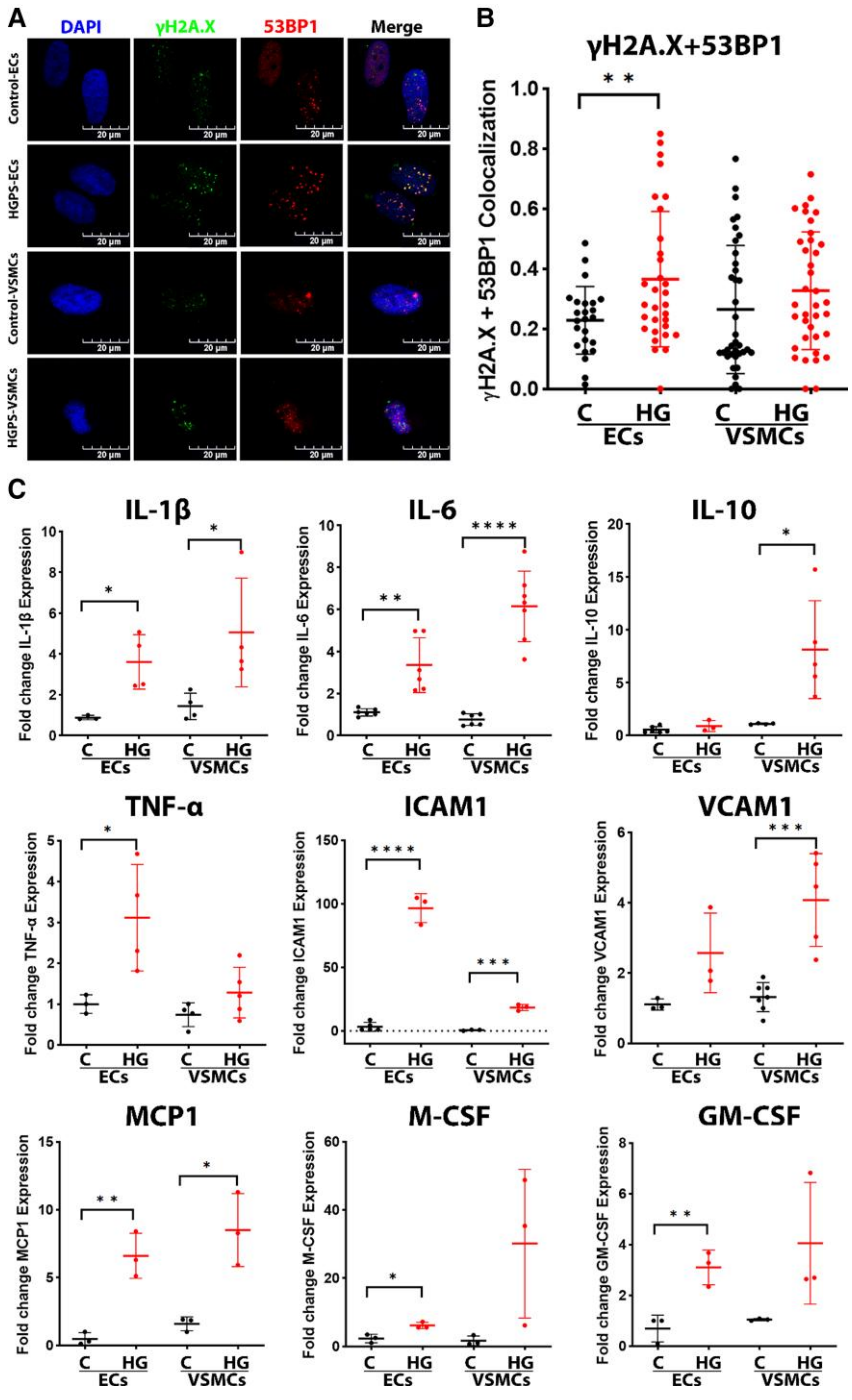

Figure 3 DNA damage, inflammation, and DNA accessibility in endothelial cells vs. vascular smooth muscle cells. (*A*) Immunofluorescence staining for DNA damage stained nuclei (DAPI, blue), γH2A.X (green), and 53BP1 (red) (scale bar: 20 μm), and quantification in (*B*) showing significantly increased colocalization of γH2A.X and 53BP1 in HGPS-ECs, in which HGPS-VSMCs not as strong; $n = 30$, replicated three times. (*C*) Quantitative reverse transcription polymerase chain reaction for inflammatory cytokines expression in both endothelial cells and vascular smooth muscle cells; $n = 3$–7. (*D*) Immunofluorescence staining for nuclei (DAPI, blue), lamin A (green), and histone H1 (red), and quantification in (*E*), showing a decrease of histone H1 in both HGPS-ECs and HGPS-VSMCs (scale bar: 20 μm). The white arrows represent cells lacking the histone H1 staining; $n = 35$. (*F*) Immunofluorescence staining for nuclei (DAPI, blue), lamin A (green), and HP1α (red), and quantification in (*G*), showing a decrease of HP1α in both HGPS-ECs and HGPS-VSMCs (scale bar: 20 μm). The white arrows represent cells that barely had HP1α staining; $n = 44$. (*H*–*J*) Western blot and quantification for histone H1 and HP1α showed a decreased expression in both HGPS-ECs and HGPS-VSMCs; $n = 3$. C, control; HGPS, Hutchinson–Gilford progeria syndrome. Statistical analysis was performed by an unpaired *t*-test when comparing two groups. A value of $P < 0.05$ was considered statistically significant. *$P < 0.05$; **$P < 0.01$; ***$P < 0.001$; ****$P < 0.0001$.

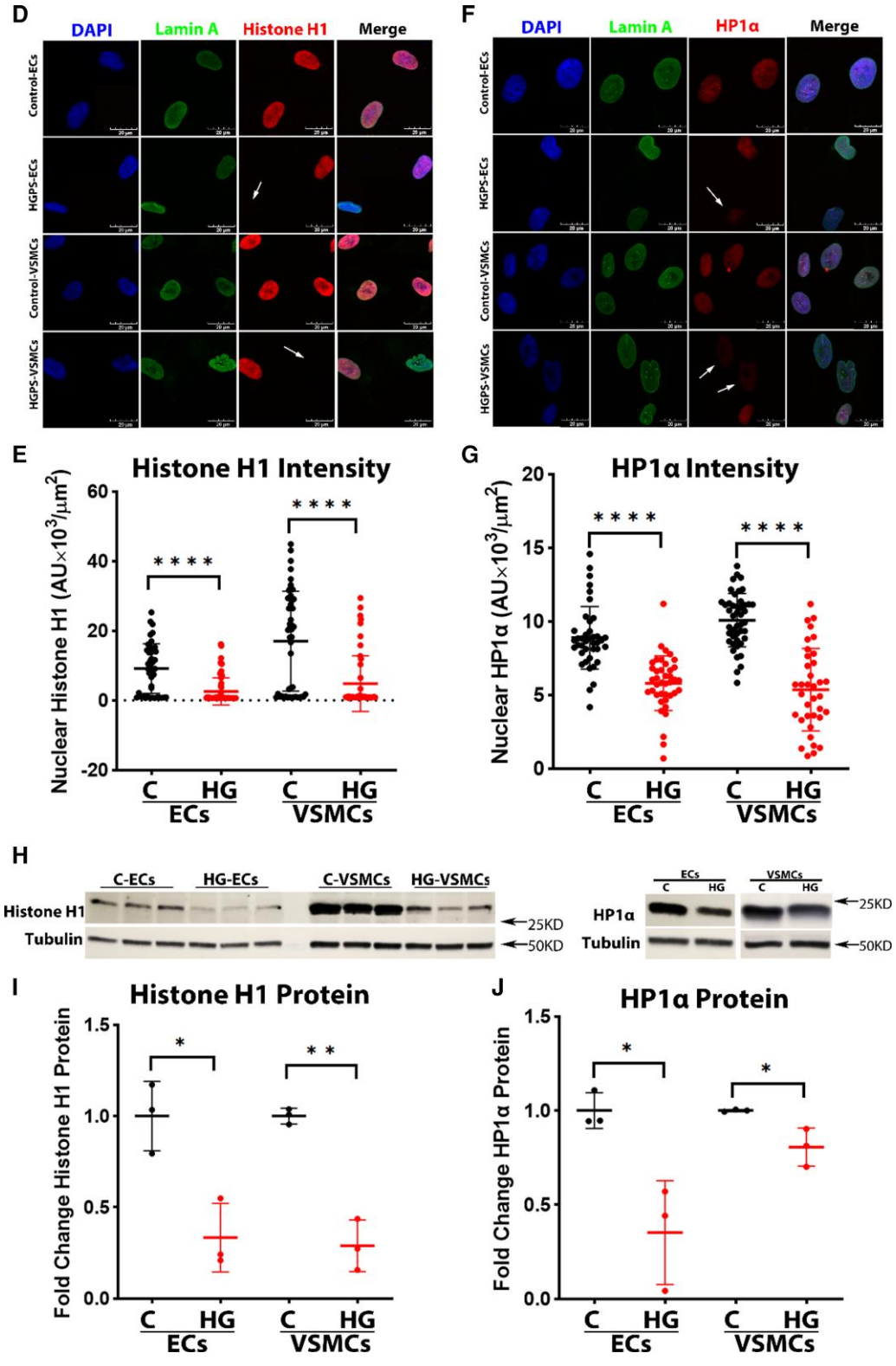

Figure 3 Continued

It is possible that the greater DNA damage in HGPS-ECs (by comparison with HGPS-VSMCs) might be due to a greater activation of inflammatory stimuli. DNA damage is associated with chronic inflammation[28] and progressive aging.[29] Accordingly, we assessed inflammatory cytokines using the Bio-Plex assay, which includes a panel of 48 inflammatory markers. As expected, SASP markers were

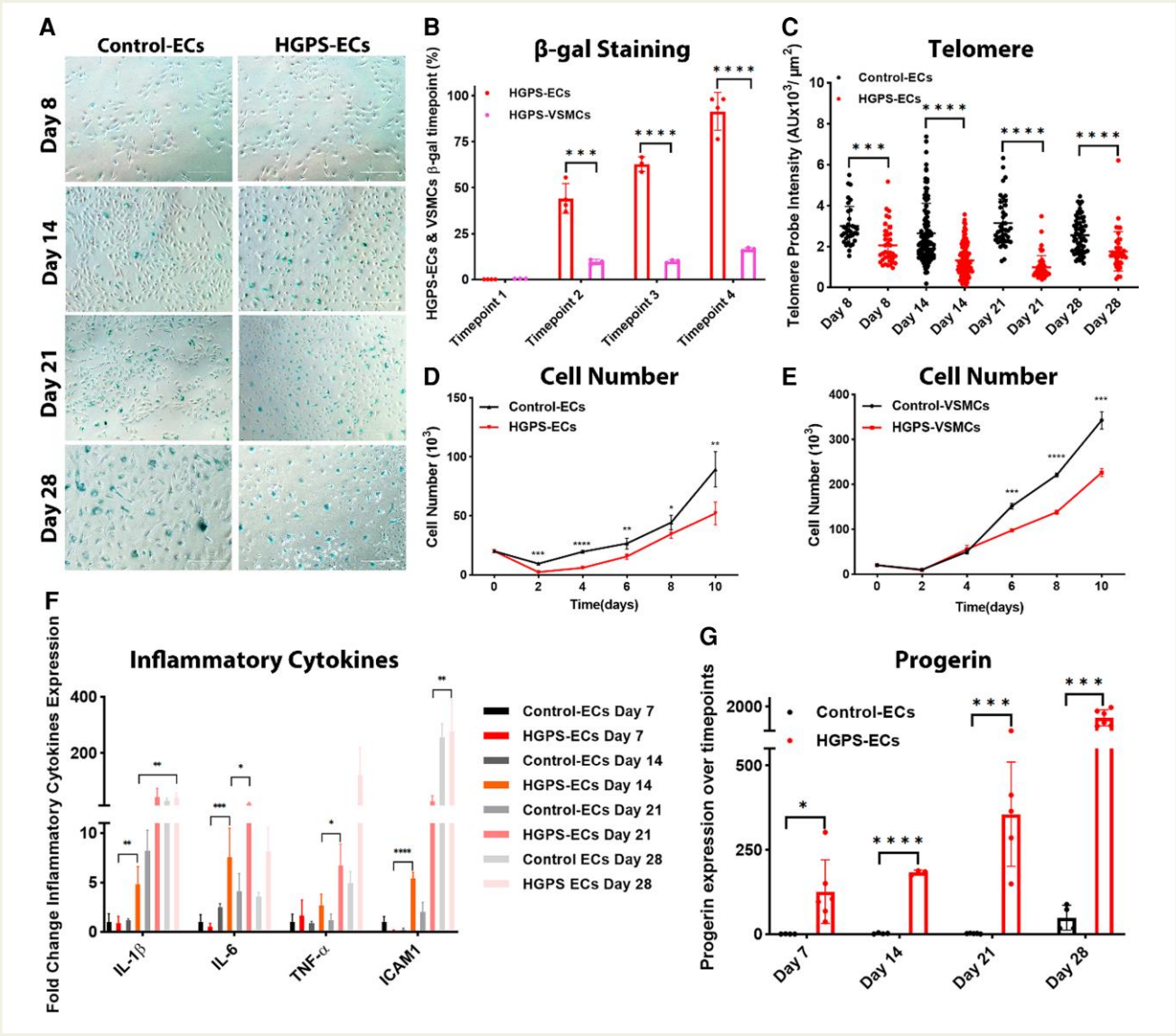

Figure 4 Aging is more accelerated in HGPS-ECs. (*A*) β-gal staining for control-ECs and HGPS-ECs on Days 8, 14, 21, and 28, showing an increasing trend over time (scale bar: 300 μm). (*B*) Quantification of β-gal staining comparing HGPS-ECs with HGPS-VSMCs at corresponding timepoints. Timepoints 1, 2, 3, and 4 represent in endothelial cells as Days 8, 14, 21, and 28 and in vascular smooth muscle cells as Days 30, 37, 44, and 51; $n = 4$. (*C*) Telomere probe intensities were normalized with nucleus area for control and HGPS-ECs on Days 8, 14, 21, and 28, $N \geq 30$ for each group. (*D*) Proliferation of endothelial cells within 10 days from both control and Hutchinson–Gilford progeria syndrome; $n = 3$. (*E*) Proliferation of vascular smooth muscle cells within 10 days from both control and Hutchinson–Gilford progeria syndrome; $n = 3$. (*F*) Quantitative reverse transcription polymerase chain reaction for inflammatory cytokines IL-1β, IL-6, TNF-α, and ICAM1 expression showed increased inflammatory cytokine expression in endothelial cells over time; $n = 3$–6. (*G*) Quantitative reverse transcription polymerase chain reaction for progerin expression over time on Days 7, 14, 21, and 28, showed a significant increase of progerin expression over time in HGPS-ECs compared with its control. $n = 4$–6. Statistical analysis was performed by an unpaired *t*-test when comparing two groups. For ≥3 groups, statistical analysis was performed using one-way analysis of variance followed by a *post hoc* Tukey's test. A value of $P<0.05$ was considered statistically significant. *$P < 0.05$; **$P < 0.01$; ***$P < 0.001$; ****$P < 0.0001$.

significantly increased in HGPS-ECs compared with their control,[16] and the same was true for HGPS-VSMCs (see Supplementary material online, *Figure S4*). To further confirm these results, we measured several well-established inflammatory markers for cardiovascular disease by RT-qPCR, a transcriptome analysis consistent with the Bio-Plex data (*Figure 3C*). These studies revealed a significant increase in inflammatory markers, such as IL-1β, IL-6, ICAM1, MCP1, in both HGPS-ECs and HGPS-VSMCs (*Figure 3C*), but no consistent difference was observed between ECs and VSMCs in terms of the magnitude of inflammatory cytokine expression.

Alternatively, the increased DNA damage in HGPS-ECs (by comparison with HGPS-VSMCs) could be due to greater DNA accessibility.[30] Thus, we assessed the markers of heterochromatin histone H1 and Hp1α by IF staining (*Figure. 3D–G*) and western blot

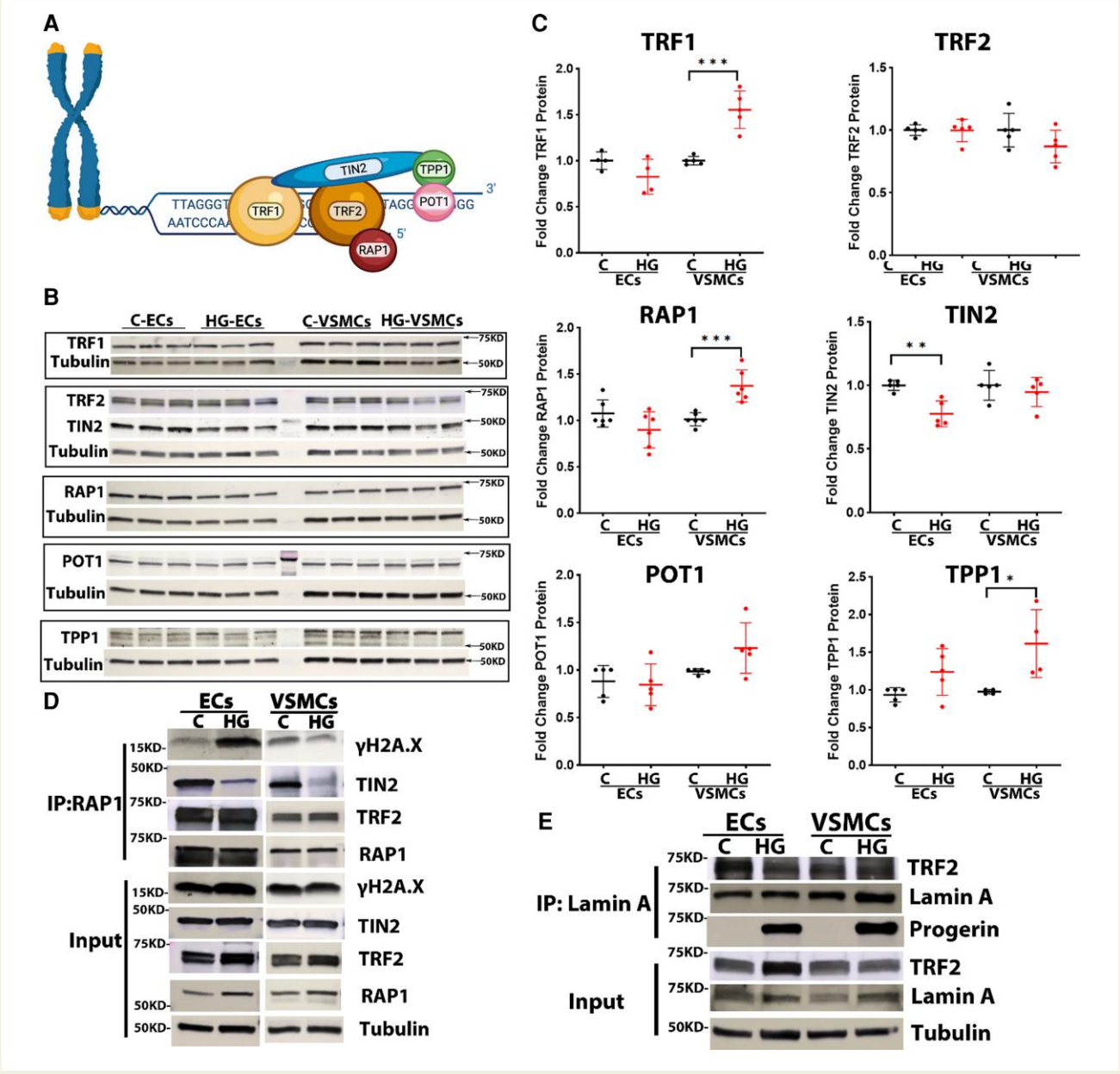

Figure 5 Alterations in the expression and interaction of shelterin protein complexes. (*A*) A schematic figure of the shelterin protein complex. (*B and C*) Western blot for six shelterin proteins and quantification in endothelial cells and vascular smooth muscle cells from both control and Hutchinson–Gilford progeria syndrome; $n = 4$–6. (*D*) Co-immunoprecipitation of γH2A.X and TIN2 with RAP1 in both endothelial cells and vascular smooth muscle cells from control and Hutchinson–Gilford progeria syndrome; $n = 3$ (*E*) Co-immunoprecipitation of TRF2 with lamin A in both endothelial cells and vascular smooth muscle cells from control and Hutchinson–Gilford progeria syndrome; $n = 3$. C, control; HGPS, Hutchinson–Gilford progeria syndrome. Statistical analysis was performed by an unpaired *t*-test when comparing two groups. A value of $P < 0.05$ was considered statistically significant. *$P < 0.05$; **$P < 0.01$; ***$P < 0.001$.

(*Figure 3H–J*). Histone H1 and Hp1α levels were reduced significantly in both HGPS-ECs and HGPS-VSMCs compared with their respective controls. Of note, histone H1 was lower in HGPS-ECs compared with HGPS-VSMCs (see Supplementary material online, *Figure S4*), consistent with the greater DNA accessibility in HGPS-ECs. Thus, in the setting of similar magnitude of inflammatory activation, HGPS-ECs fare worse than HGPS-VSMCs possibly due to the increased DNA accessibility allowing for greater susceptibility to DNA damage.

Aging is more accelerated in HGPS-ECs

To determine whether aging is more accelerated in HGPS-ECs than in HGPS-VSMCs, we examined the effect of passaging cells for 28 days on senescence progression as assessed by β-gal expression (*Figure 4A and B*; see Supplementary material online, *Figure S5*), telomere length (*Figure 4C*; see Supplementary material online, *Figure S5*), and cellular proliferation (*Figure 4D and E*) and compared each with their respective controls. Intriguingly, the progression of senescence

was accelerated in HGPS-ECs by comparison with HGPS-VSMCs. In HGPS-ECs, we observed a significant increase in the percentage of β-gal positive cells and a significant reduction in telomere length in HGPS-ECs compared with control-ECs throughout the 28-day period. Surprisingly, although the telomere length in HGPS-VSMCs shortened over time, we did not observe similar severity in the senescence of HGPS-VSMCs as indicated by the β-gal staining. To understand whether the higher progressive senescence in HGPS-ECs compared with HGPS-VSMCs was related to cellular proliferation, we counted cells within 10 days in both ECs and VSMCs after seeding an equal number of cells on Day 0. To our surprise, both control-VSMCs and HGPS-VSMCs proliferated more than control-ECs and HGPS-ECs, and the number of HGPS-VSMCs were higher than HGPS-ECs on Day 10 (*Figure 4D and E*). Hence, cell proliferation *in vitro* is reduced in ECs by comparison with isogenic VSMCs. To better understand the senescent phenotype of HGPS-ECs, we investigated SASP markers and progerin in ECs in a time-course experiment. Indeed, we found the SASP markers to be consistently higher over time in HGPS-ECs by comparison with control-ECs after Day 7 (*Figure 4F*) and progerin to be significantly higher in HGPS-ECs over time (*Figure 4G*). In conclusion, HGPS-ECs age faster than HGPS-VSMCs, despite proliferating to a lesser extent than HGPS-VSMCs.

Alterations in the expression and interaction of SPC proteins

To investigate whether significantly shorter telomeres in HGPS-ECs and HGPS-VSMCs were due to alterations in the expression and interactions of SPC proteins, we examined all six members of the SPC (TRF1, TRF2, RAP1, TIN2, POT1, and TPP1) (*Figure 5A*) at the mRNA and protein levels (see Supplementary material online, *Figure S6*; *Figure 5B and C*). After assessing the mRNA and protein levels of each SPC protein, we focused on RAP1 due to its consistent pattern of expression in both ECs and VSMCs. RAP1 is critical to the SPC because a deficiency of RAP1 leads to telomere fusion and senescence.[31,32] We performed IP for RAP1 followed by Mass Spectrometry (MS) for control-ECs and HGPS-ECs. Our data showed a strong association of TRF2 to RAP1 in both control-ECs and HGPS-ECs as expected. However, to our surprise, RAP1 lost its association with TIN2 in HGPS-ECs (see Supplementary material online, *Figure S6*), while its connection was preserved in control-ECs. We then conducted RAP1-IP followed by western blot to confirm the MS analysis. The binding of TIN2 to RAP1 through TRF2 was reduced in both HGPS-ECs and HGPS-VSMCs compared with their respective controls (*Figure 5D*). TIN2 serves as a bridge between TRF1/TRF2/RAP1 and TPP1/POT1 to form the intact SPC.[33] Since we observed increased DNA damage in HGPS cells (*Figure 3A and B*), we investigated the possible role of DNA damage contributing to the dissociation of TIN2 from RAP1. Thus, we probed for γH2A.X in RAP1-IP samples of both ECs and VSMCs. Our results demonstrated strong signals of γH2A.X binding to RAP1 in HGPS-ECs but not in HGPS-VSMCs (*Figure 5D*).

It was previously shown that TRF2 binding to lamin A is disrupted in HGPS fibroblasts.[34] To understand whether the loss of TRF2 binding to lamin A also exerted a synergistic effect with a reduction of TIN2 binding to RAP1 to further impair SPC interactions, we performed Lamin A-IP and probed for TRF2. As expected, we observed a significant reduction of TRF2 binding to lamin A (progerin) in HGPS-ECs compared with control0ECs (*Figure 5E*); however, in HGPS-VSMCs, reduced TRF2 binding was not significant. In conclusion, these data demonstrate a reduction of TIN2 binding to RAP1 through TRF2, together with a disassociation of TRF2 with lamin A, which is associated with increased DNA damage. These alterations in the SPC may contribute to telomere attrition and cellular senescence, most prominently in HGPS-ECs.

Discussion

Our study is the first to characterize and to compare in parallel the functions of human HGPS-ECs and HGPS-VSMCs. This study reveals that the endothelial abnormality in HGPS is more severe than that in VSMCs. Furthermore, this study directs attention to the defect in the endothelium as a critical determinant of the vascular pathobiology in HGPS. In addition, we extend this new understanding by investigating the mechanisms of DNA damage in HGPS vascular cells. The endothelial dysfunction described herein may play a critical role in the initiation and progression of the arterial occlusive disease of HGPS.[5,7]

Several mouse models have been generated to replicate the phenotypes of HGPS patients.[35,36] These models phenocopy many progeria traits such as alopecia, loss of subcutaneous fat, loss of weight, reduced height, and skeletal dysplasia.[37] However, most models are deficient in generating the coronary and carotid arterial occlusive disease, which are features of HGPS children. The vascular abnormality observed in most mouse models of HGPS is an extensive VSMC loss in the media.[12] As a result, most researchers in this field studying the vascular disease in progeria have focused on VSMCs with less emphasis on ECs.

This peculiar focus on VSMCs looks past the finding that in humans, the mortality in progeria is not due to thinning of the media, but rather due to arterial occlusive disease in the coronary and carotid arteries. *Generally, arterial occlusive disease of the coronary and carotid artery disease in humans begins with an endothelial dysfunction.*[13,14] Endothelial dysfunction is a strong determinant of vascular disease because endothelial homeostasis is critical for vascular patency.[38] By virtue of its production of a panoply of paracrine factors, the endothelium regulates the proliferation and tone of the underlying vascular smooth muscle.[14] As a consequence of its interposition between the blood and the vessel wall, the endothelium regulates the interaction of circulating blood elements within the vessel. In health, the endothelium acts as the Teflon lining of the vessel, preventing adherence and aggregation of platelets, and infiltration of leucocytes.[13] Alterations in endothelial homeostasis can lead to vasoconstriction, thrombosis, and inflammation.[39] Chronic endothelial dysfunction underlies the progression of vascular disease and major adverse cardiovascular events.[40]

Indeed, the attrition of the media that is seen in HGPS could be due to an endothelial defect. We have previously shown that HGPS-ECs have a proteomic profile consistent with SASP.[16] Intriguingly, this proteomic profile of senescence is partially reversed by the treatment of the HGPS EC with mRNA encoding human telomerase (hTERT). When control-VSMCs were subject to the various conditioned media,

their proliferation was greatly reduced when cultured with the HGPS EC–conditioned media, but proliferation was not affected when cultured using media from control-ECs or with media from HGPS-ECs treated with hTERT. Bio-Plex analysis of VSMCs exposed to different conditioned media demonstrated that VSMCs themselves also secreted more inflammatory markers when cultured with HGPS EC donor media, though this shift was attenuated when hTERT-treated HGPS-ECs were the donor. These data provide further support for our hypothesis that a severe loss of endothelial homeostasis may be primarily responsible for the vascular pathology observed in HGPS, including the attenuation of the vascular media.

There has been some prior work to characterize the endothelial alterations in HGPS. In a cellular model of progeria, healthy primary ECs and progenitors from human umbilical vein or cord blood were cultured and treated with the protease inhibitor (Atazanavir) to induce the accumulation of farnesylated prelamin A. This effect was associated with nuclear shape abnormalities, inflammatory activation and increased adhesiveness for monocytes, and impaired angiogenesis and pre-mature senescence in both differentiated and progenitor ECs.[41] In the *Prog-Tg* HGPS mouse model, endothelial-specific progerin expression is associated with impaired shear stress response, reduced levels of endothelial nitric oxide synthase (eNOS) expression, NO generation, and impaired mechanosignaling.[42]

The preponderance of published studies has focused on the effects of progerin on VSMCs,[43] with less investigation on ECs. However, one group investigated ECs and VSMCs in tissue-engineered blood vessels (TEBVs) and identified that HGPS-ECs were less responsive to shear stress, with impaired up-regulation of KLF2, Nrf2, and eNOS and reduced vasodilation to acetylcholine.[43] This comparison was done in a similar manner as in this paper as the cells were compared following differentiation. In this work, HGPS-VSMCs manifested less contractile protein expression and impaired contractility. Intriguingly, when normal ECs or VSMCs were substituted in the TEBV for their HGPS counterpart, those TEBV with HGPS-ECs had greater impairment in vasoreactivity and inflammatory markers than TEBV with HGPS-VSMCs. Thus, HGPS-ECs had a greater effect on TEBV impairment than did HGPS-VSMCs in this work. Additionally, Bersini and colleagues reprogrammed normal or HGPS fibroblasts into induced VSMCs (iVSMCs) and induced vascular endothelial cells (iVECs). They found that when co-cultured with ECs in a microfluidic device, HGPS iVSMCs increased vascular permeability, an effect attributed in part to the increased expression of BMP4 and Jagged 1 in the HGPS iVSMCs.[44]

Whether coronary and carotid artery disease in progeria children follows the well-characterized progression of the more common form of atherosclerotic arterial occlusive disease is not known. Nevertheless, arterial occlusive disease in children with progeria shares more similarities to atherosclerosis in adult humans than it does to the vascular disease in HGPS mice.[10] Therefore, our study of the isogenic lines of HGPS-ECs and HGPS-VSMCs is an important step towards understanding the mechanisms of arterial occlusive disease in progeria. Our work suggests that the functional alterations in HGPS-ECs are as severe or more so in HGPS-VSMCs. Furthermore, HGPS-ECs appear to age more rapidly than HGPS-VSMCs *in vitro*, as manifested by significantly increased β-gal staining over the same time-course. This difference in aging may be related to cell lineage, as normal ECs also seemed to age faster than normal vascular smooth muscle cells in culture. Regardless, if there is such a differential cellular response to time on cellular aging, any vascular alteration in HGPS will be more pronounced in the endothelium. Thus, an endothelial-targeted therapy may have great benefit in HGPS. Indeed, we have recently shown that the treatment of HGPS mice with intravenous injection of a lentiviral construct encoding murine telomerase improved endothelial functions, with minimal effect on the medial VSMCs, yet increased longevity.[16]

The shortened telomere length in HGPS cells may be explained by increased DNA damage or loss of protection by impaired interactions of the SPC members. TIN2 is a critical protein of SPC as it connects the complex by joining TRF1/TRF2/RAP1 (which binds to double-stranded DNA), with TPP1/POT1 (which binds to single-stranded DNA).[45] Based on our MS data analysis of proteins isolated by RAP1-IP, the interaction between TIN2 and RAP1 through TRF2 decreased in both HGPS-ECs and HGPS-VSMCs. Interestingly, the binding of RAP1 and γH2A.X was significantly increased only in HGPS-ECs but not in HGPS-VSMCs. The interaction between γH2A.X and RAP1 may be a manifestation of greater DNA damage and telomere erosion in HGPS-ECs. The TIN2 binding to RAP1, through TRF2, was compromised in both HGPS-ECs and HGPS-VSMCs compared with their respective controls, together with a shortened telomere length in HGPS cells, suggesting the important role of TIN2–TRF2–RAP1 interactions in protecting telomere ends. TIN2 has been shown to stabilize the binding of TRF2 to double-stranded telomeric DNAs, which is a crucial function of the shelterin complex to protect the telomeric ends.[45,46] Additionally, the reduction of TIN2 causes DNA damage at the telomeres, but the DNA damage was prevented following an induced expression of TIN2.[46,47]

Additionally, RAP1 binds to TRF2, linking the shelterin protein complex to the telomere and protecting it from DNA damage.[48] In addition, TRF2 binds to lamin A.[34] Our lamin A pulldown revealed a reduction in TRF2 binding only in HGPS-ECs. It is possible that a greater impairment of the shelterin protein complex interactions in HGPS-ECs accounts for their greater telomere erosion and senescence markers. Alternatively, the increase in the expression of several shelterin protein complex components in HGPS-VSMCs (TRF1, RAP1, and TPP1) may have compensated for the impaired shelterin interaction, reducing the senescence process induced by progerin. Alternatively, or in addition, the greater DNA damage in HGPS-ECs may be related to greater DNA accessibility in the setting of inflammatory activation. In this regard, greater DNA damage is observed in progerin-overexpressing human dermal fibroblasts during the S phase when heterochromatin is reduced.[49] To summarize, the evidence of more advanced senescence in HGPS-ECs (by comparison with HGPS-VSMCs) may be due to greater DNA accessibility to DNA damage, in part due to a greater impairment in SPC interactions.

A limitation of our study is that only one HGPS cell line and its corresponding parental cell line were used in this study. However, we and others have shown that different HGPS-iPSC cell lines are quite similar in terms of pluripotency, transcriptional and epigenetic profiles, and capability for differentiation towards all three germ layers.[17] However, the differentiated cells from HGPS patients can have different severities of progeria phenotype as we have previously shown.[50] Moreover, the culture conditions for ECs and SMCs derived from iPSC were different. However, the culture conditions that we used are well-established and optimized for cell type.

Accordingly, it is unlikely that this difference in culture conditions is responsible for the differential effect of progeria on cell function. Nevertheless, these are quantitative differences between cell lines, not qualitative differences, and thus unlikely to alter the conclusions of this paper.

Our findings may be more broadly relevant to the general population, as progerin is expressed at low levels in normal individuals and accumulates in the vessel wall as we age.[50] Furthermore, many of the processes contributing to accelerated aging in HGPS—inflammatory activation, telomere erosion, loss of heterochromatin, increased DNA damage—are involved in normal aging. Understanding these mechanisms in HGPS may guide us in developing senomodulatory strategies for healthy aging.[22,51]

Lead author biography

Qiu Xu, a medical student at Central South University, Xiangya School of Medicine. She is currently in an exchange program at Methodist Research Institute. Her research interests include cardiovascular regeneration, cardiovascular disease in progeria, and hTERT treatment in cardiovascular disease.

Anahita Mojiri, PhD, Instructor, Houston Methodist Research Institute (HMRI). Her research is focused on molecular and cellular senescent of vascular system. Her work indicates that hTERT mRNA therapy might be a promising approach for HGPS and other age-related vascular diseases.

Author contributions

Q.X. and A.M. equally contributed to the design and performance of experiments. Q.X. performed the detailed analysis of data, with assistance of L.B., who also designed the graphical abstract. E.M. generated and analysed the confocal microscopy figures. B.W. performed and analysed MMqPCR. Q.X., A.M., L.B., E.M., and J.C. wrote the manuscript. All authors contributed to editing the manuscript. J.C. oversaw all aspects of the research, contributed to the design of the experiments and their analysis, generated multiple revisions of the manuscript, was primarily responsible for the written response to the reviewers, and funded the study.

Data availability

The data that support the findings of this study are available from the corresponding author upon reasonable request.

Supplementary material

Supplementary material is available at *European Heart Journal Open* online.

Acknowledgements

We acknowledge Anna Malovannaya for her primary analysis of MS data. We acknowledge BCM Mass Spectrometry Proteomics Core, which is supported by the Dan L. Duncan Comprehensive Cancer Center NIH award (P30 CA125123) and CPRIT Core Facility Award (RP170005). We acknowledge Nicole Vaughn for her help with sorting cells. This work would not be possible without the Progeria Research Foundation (PRF) Cell and Tissue Bank, which supplied the HGPS cell lines used in this study.

Funding

This work is supported by grants to JPC [National Institutes of Health (NIH) R01s HL133254 and HL148338; as well as the Cancer Prevention and Research Institute of Texas CPRIT RP150611].

Conflict of interest: Dr. Cooke is an inventor on patents owned by Stanford University and Houston Methodist Hospital related to the use of mRNA telomerase for the treatment of senescence, which intellectual property has been licensed in part to ChromeX Bio, in which company Dr. Cooke has equity.

References

1. Eriksson M, Brown WT, Gordon LB, Glynn MW, Singer J, Scott L, Erdos MR, Robbins CM, Moses TY, Berglund P, Dutra A, Pak E, Durkin S, Csoka AB, Boehnke M, Glover TW, Collins FS. Recurrent de novo point mutations in lamin A cause Hutchinson–Gilford progeria syndrome. *Nature* 2003;**423**:293–298.
2. Cenni V, Capanni C, Mattioli E, Schena E, Squarzoni S, Bacalini MG, Garagnani P, Salvioli S, Franceschi C, Lattanzi G. Lamin A involvement in ageing processes. *Ageing Res Rev* 2020;**62**:101073.
3. Taimen P, Pfleghaar K, Shimi T, Moller D, Ben-Harush K, Erdos MR, Adam SA, Herrmann H, Medalia O, Collins FS, Goldman AE, Goldman RD. A progeria mutation reveals functions for lamin A in nuclear assembly, architecture, and chromosome organization. *Proc Natl Acad Sci U S A* 2009;**106**:20788–20793.
4. Musich PR, Zou Y. DNA-damage accumulation and replicative arrest in Hutchinson-Gilford progeria syndrome. *Biochem Soc Trans* 2011;**39**:1764–1769.
5. Ullrich NJ, Gordon LB. Hutchinson-Gilford progeria syndrome. *Handb Clin Neurol* 2015;**132**:249–264.
6. Gonzalo S, Kreienkamp R, Askjaer P. Hutchinson-Gilford progeria syndrome: A premature aging disease caused by LMNA gene mutations. *Ageing Res Rev* 2017;**33**: 18–29.
7. Merideth MA, Gordon LB, Clauss S, Sachdev V, Smith AC, Perry MB, Brewer CC, Zalewski C, Kim HJ, Solomon B, Brooks BP, Gerber LH, Turner ML, Domingo DL, Hart TC, Graf J, Reynolds JC, Gropman A, Yanovski JA, Gerhard-Herman M, Collins FS, Nabel EG, Cannon RO, Gahl WA, Introne WJ. Phenotype and course of Hutchinson-Gilford progeria syndrome. *N Engl J Med* 2008;**358**:592–604.
8. Stehbens WE, Wakefield SJ, Gilbert-Barness E, Olson RE, Ackerman J. Histological and ultrastructural features of atherosclerosis in progeria. *Cardiovasc Pathol* 1999; **8**:29–39.
9. Stehbens WE, Delahunt B, Shozawa T, Gilbert-Barness E. Smooth muscle cell depletion and collagen types in progeric arteries. *Cardiovasc Pathol* 2001;**10**:133–136.
10. Hamczyk MR, Villa-Bellosta R, Gonzalo P, Andres-Manzano MJ, Nogales P, Bentzon JF, López-Otín C, Andrés V. Vascular smooth muscle-specific progerin expression accelerates atherosclerosis and death in a mouse model of Hutchinson-Gilford progeria syndrome. *Circulation* 2018;**138**:266–282.
11. Del Campo L, Sanchez-Lopez A, Gonzalez-Gomez C, Andres-Manzano MJ, Dorado B, Andres V. Vascular smooth muscle cell-specific progerin expression provokes contractile impairment in a mouse model of Hutchinson-Gilford progeria syndrome that is ameliorated by nitrite treatment. *Cells* 2020;**9**: 656.
12. Varga R, Eriksson M, Erdos MR, Olive M, Harten I, Kolodgie F, Capell BC, Cheng J, Faddah D, Perkins S, Avallone H, San H, Qu X, Ganesh S, Gordon LB, Virmani R, Wight TN, Nabel EG, Collins FS. Progressive vascular smooth muscle cell defects in a mouse model of Hutchinson-Gilford progeria syndrome. *Proc Natl Acad Sci U S A* 2006;**103**:3250–3255.

13. Harker LA, Schwartz SM, Ross R. Endothelium and arteriosclerosis. *Clin Haematol* 1981;**10**:283–296.
14. Cooke JP, Dzau VJ. Nitric oxide synthase: role in the genesis of vascular disease. *Ann Rev Med* 1997;**48**:489–509.
15. Yu XH, Fu YC, Zhang DW, Yin K, Tang CK. Foam cells in atherosclerosis. *Clin Chim Acta* 2013;**424**:245–252.
16. Mojiri A, Walther BK, Jiang C, Matrone G, Holgate R, Xu Q, Morales E, Wang G, Gu J, Wang R, Cooke JP. Telomerase therapy reverses vascular senescence and extends lifespan in progeria mice. *Eur Heart J* 2021;**42**:4352–4369.
17. Chen Z, Chang WY, Etheridge A, Strickfaden H, Jin Z, Palidwor G, Cho J-H, Wang K, Kwon SY, Doré C, Raymond A, Hotta A, Ellis J, Kandel RA, Dilworth FJ, Perkins TJ, Hendzel MJ, Galas DJ, Stanford WL. Reprogramming progeria fibroblasts re-establishes a normal epigenetic landscape. *Aging Cell* 2017;**16**:870–887.
18. Matrone G, Thandavarayan RA, Walther BK, Meng S, Mojiri A, Cooke JP. Dysfunction of iPSC-derived endothelial cells in human Hutchinson-Gilford progeria syndrome. *Cell Cycle* 2019;**18**:2495–2508.
19. Cai Y, Sukhova GK, Wong HK, Xu A, Tergaonkar V, Vanhoutte PM, Tang EHC. Rap1 induces cytokine production in pro-inflammatory macrophages through NFkappaB signaling and is highly expressed in human atherosclerotic lesions. *Cell Cycle* 2015;**14**:3580–3592.
20. Goldman RD, Shumaker DK, Erdos MR, Eriksson M, Goldman AE, Gordon LB, Gruenbaum Y, Khuon S, Mendez M, Varga R, Collins FS. Accumulation of mutant lamin A causes progressive changes in nuclear architecture in hutchinson–gilford progeria syndrome. *Proc Natl Acad Sci U S A* 2004;**101**:8963–8968.
21. Bernadotte A, Mikhelson VM, Spivak IM. Markers of cellular senescence. Telomere shortening as a marker of cellular senescence. *Aging* 2016;**8**:3–11.
22. López-Otín C, Blasco MA, Partridge L, Serrano M, Kroemer G. The hallmarks of aging. *Cell* 2013;**153**:1194–1217.
23. Chojnowski A, Ong PF, Wong ES, Lim JS, Mutalif RA, Navasankari R, Dutta B, Yang H, Liow YY, Sze SK, Boudier T, Wright GD, Colman A, Burke B, Stewart CL, Dreesen O. Progerin reduces LAP2α-telomere association in Hutchinson-Gilford progeria. *eLife* 2015;**4**:e07759.
24. Dimri GP, Lee X, Basile G, Acosta M, Scott G, Roskelley C, Medrano E E, Linskens M, Rubelj I, Pereira-Smith O. A biomarker that identifies senescent human cells in culture and in aging skin in vivo. *Proc Natl Acad Sci U S A* 1995;**92**:9363–9367.
25. Lombard DB, Chua KF, Mostoslavsky R, Franco S, Gostissa M, Alt FW. DNA Repair, genome stability, and aging. *Cell* 2005;**120**:497–512.
26. Yousefzadeh M, Henpita C, Vyas R, Soto-Palma C, Robbins P, Niedernhofer L. DNA damage-how and why we age? *Elife* 2021;**10**:e62852.
27. Pitrez PR, Estronca L, Monteiro LM, Colell G, Vazao H, Santinha D, Harhouri K, Thornton D, Navarro C, Egesipe A-L, Carvalho T, Dos Santos RL, Lévy N, Smith JC, de Magalhães JP, Ori A, Bernardo A, De Sandre-Giovannoli A, Nissan X, Rosell A, Ferreira L. Vulnerability of progeroid smooth muscle cells to biomechanical forces is mediated by MMP13. *Nat Commun* 2020;**11**:4110.
28. Kawanishi S, Ohnishi S, Ma N, Hiraku Y, Murata M. Crosstalk between DNA damage and inflammation in the multiple steps of carcinogenesis. *Int J Mol Sci* 2017;**18**:1808.
29. Schumacher B, Pothof J, Vijg J, Hoeijmakers JHJ. The central role of DNA damage in the ageing process. *Nature* 2021;**592**:695–703.
30. Di Micco R, Sulli G, Dobreva M, Liontos M, Botrugno OA, Gargiulo G, dal Zuffo R, Matti V, d'Ario G, Montani E, Mercurio C, Hahn WC, Gorgoulis V, Minucci S, d'Adda di Fagagna F. Interplay between oncogene-induced DNA damage response and heterochromatin in senescence and cancer. *Nat Cell Biol* 2011;**13**:292–302.
31. Lototska L, Yue JX, Li J, Giraud-Panis MJ, Songyang Z, Royle NJ, Liti G, Ye J, Gilson E, Mendez-Bermudez A. Human RAP1 specifically protects telomeres of senescent cells from DNA damage. *EMBO Rep* 2020;**21**:e49076.
32. Rai R, Chen Y, Lei M, Chang S. TRF2-RAP1 Is required to protect telomeres from engaging in homologous recombination-mediated deletions and fusions. *Nat Commun* 2016;**7**:10881.
33. Diotti R, Loayza D. Shelterin complex and associated factors at human telomeres. *Nucleus* 2011;**2**:119–135.
34. Wood AM, Rendtlew Danielsen JM, Lucas CA, Rice EL, Scalzo D, Shimi T, Goldman RD, Smith ED, Le Beau MM, Kosak ST. TRF2 And lamin A/C interact to facilitate the functional organization of chromosome ends. *Nat Commun* 2014;**5**:5467.
35. Mayoral P, Bárcena C, López-Otín C. Progeria mouse models. In: *Conn's handbook of models for human aging*. 2018. p. 689–701.
36. Carrero D, Soria-Valles C, López-Otín C. Hallmarks of progeroid syndromes: lessons from mice and reprogrammed cells. *Dis Model Mech* 2016;**9**:719–735.
37. Zaghini A, Sarli G, Barboni C, Sanapo M, Pellegrino V, Diana A, Linta N, Rambaldi J, D'Apice MR, Murdocca M, Baleani M, Baruffaldi F, Fognani R, Mecca R, Festa A, Papparella S, Paciello O, Prisco F, Capanni C, Loi M, Schena E, Lattanzi G, Squarzoni S. Long term breeding of the lmna G609G progeric mouse: characterization of homozygous and heterozygous models. *Exp Gerontol* 2020;**130**:110784.
38. Cooke JP. Flow, NO, and atherogenesis. *Proc Natl Acad Sci U S A* 2003;**100**:768–770.
39. Ross R. Atherosclerosis—an inflammatory disease. *N Eng J Med* 1999;**340**:115–126.
40. Wilson AM, Shin DS, Weatherby C, Harada RK, Ng MK, Nair N, Kielstein J, Cooke J. Asymmetric dimethylarginine correlates with measures of disease severity, major adverse cardiovascular events and all-cause mortality in patients with peripheral arterial disease. *Vasc Med* 2010;**15**:267–274.
41. Bonello-Palot N, Simoncini S, Robert S, Bourgeois P, Sabatier F, Levy N, Dignat-George F, Badens C. Prelamin A accumulation in endothelial cells induces premature senescence and functional impairment. *Atherosclerosis* 2014;**237**:45–52.
42. Osmanagic-Myers S, Kiss A, Manakanatas C, Hamza O, Sedlmayer F, Szabo PL, Fischer I, Fichtinger P, Podesser BK, Eriksson M, Foisner R. Endothelial progerin expression causes cardiovascular pathology through an impaired mechanoresponse. *J Clin Invest* 2019;**129**:531–545.
43. Atchison L, Abutaleb NO, Snyder-Mounts E, Gete Y, Ladha A, Ribar T, Cao K, Truskey GA. iPSC-derived endothelial cells affect vascular function in a tissue-engineered blood vessel model of Hutchinson-Gilford progeria syndrome. *Stem Cell Rep* 2020;**14**:325–337.
44. Bersini S, Schulte R, Huang L, Tsai H, Hetzer MW. Direct reprogramming of human smooth muscle and vascular endothelial cells reveals defects associated with aging and Hutchinson-Gilford progeria syndrome. *Elife* 2020;**9**:e54383.
45. Hu C, Rai R, Huang C, Broton C, Long J, Xu Y, Xue J, Lei M, Chang S, Chen Y. Structural and functional analyses of the mammalian TIN2-TPP1-TRF2 telomeric complex. *Cell Res* 2017;**27**:1485–1502.
46. Frescas D, de Lange T. TRF2-tethered TIN2 can mediate telomere protection by TPP1/POT1. *Mol Cell Biol* 2014;**34**:1349–1362.
47. Frescas D, de Lange T. Binding of TPP1 protein to TIN2 protein is required for POT1a, b protein-mediated telomere protection. *J Biol Chem* 2014;**289**:24180–24187.
48. Lototska L, Yue JX, Li J, Giraud-Panis MJ, Songyang Z, Royle NJ, Liti G, Ye J, Gilson E, Mendez-Bermudez A. Human RAP 1 specifically protects telomeres of senescent cells from DNA damage. *EMBO Rep* 2020;**21**:e49076.
49. Chojnowski A, Ong PF, Foo MXR, Liebl D, Hor LP, Stewart CL, Dreesen O. Heterochromatin loss as a determinant of progerin-induced DNA damage in hutchinson–gilford progeria. *Aging Cell* 2020;**19**:e13108.
50. Olive M, Harten I, Mitchell R, Beers JK, Djabali K, Cao K, Erdos MR, Blair C, Funke B, Smoot L, Gerhard-Herman M, Machan JT, Kutys R, Virmani R, Collins FS, Wight TN, Nabel EG. Cardiovascular pathology in Hutchinson-Gilford progeria: correlation with the vascular pathology of aging. *Arterioscler Thromb Vasc Biol* 2010;**30**:2301–2309.
51. Kubben N, Misteli T. Shared molecular and cellular mechanisms of premature ageing and ageing-associated diseases. *Nat Rev Mol Cell Biol* 2017;**18**:595–609.